Developing a wind turbine planning platform

Integration of “sound propagation model–GIS-game engine” triplet

Rafiee, Azarakhsh; Van der Male, Pim; Dias, Eduardo; Scholten, Henk

DOI
10.1016/j.envsoft.2017.06.019

Publication date
2017

Document Version
Final published version

Published in
Environmental Modelling & Software

Citation (APA)
Rafiee, A., Van der Male, P., Dias, E., & Scholten, H. (2017). Developing a wind turbine planning platform: Integration of “sound propagation model–GIS-game engine” triplet. *Environmental Modelling & Software*, *95*, 326-343. https://doi.org/10.1016/j.envsoft.2017.06.019

Environmental Modelling & Software 95 (2017) 326–343

Contents lists available at ScienceDirect

Environmental Modelling & Software

journal homepage: www.elsevier.com/locate/envsoft

Developing a wind turbine planning platform: Integration of "sound propagation model–GIS-game engine" triplet

Azarakhsh Rafiee [a, c, *], Pim Van der Male [b], Eduardo Dias [a, c], Henk Scholten [a, c]

[a] Department of Spatial Economics/SPINlab, VU University Amsterdam, De Boelelaan 1105, 1081 HV Amsterdam, The Netherlands
[b] Department of Hydraulic Engineering, Delft University of Technology, Mekelweg 2, 2628 CN Delft, The Netherlands
[c] Geodan Research Department, President Kennedylaan 1, 1079MB Amsterdam, The Netherlands

ARTICLE INFO

Article history:
Received 22 November 2016
Received in revised form
29 April 2017
Accepted 15 June 2017
Available online 29 June 2017

Keywords:
Wind turbine planning
Game engine
GIS
Sound propagation model
OGC standard protocols
Real-time scenario analysis

ABSTRACT

In this study, we propose an interactive information system for wind turbine siting, considering its visual and sound externalities. This system is an integration of game engine, GIS and analytical sound propagation model in a unified 3D web environment. The game engine–GIS integration provides a 3D virtual environment where users can navigate through the existing geospatial data of the whole country and place different wind turbine types to explore their visual impact on the landscape. The integration of a sound propagation model in the game engine–GIS supports the real-time calculation and feedback regarding wind turbine sound at the surrounding buildings. The platform's GIS component enables massive (on-the-fly) georeferenced data utilization through tiling techniques as well as data accessibility and interoperability via cloud-based architecture and open geospatial standard protocols. The game engine, on the other hand, supports performance optimization for both data display and sound model calculations.

Software availability

Software name: Geodan Falcon
Developers: Nils Citoulex (till 2014), Tim Ebben, Azarakhsh Rafiee, Steven Bos and Bert Temme
Hardware requirements: SSE2 instruction set support, DX9 (shader model 2.0) capabilities
Software requirements: Internet Browser that supports plugins (tested with Internet Explorer (V ≥ 9) and Firefox) and Unity Web Player Plugin (for the web player version)
Programming language: C#
Applied libraries: GeoAPI[1], GeoJSON.Net[2], Newtonsoft.Json[3], DotNetZip [4], Proj4Net[5], Pngcs[6], UnityEngine[7]. Net2.0[8]
Software language: English, Dutch
Availability: Freely available

1. Introduction

1.1. Wind energy: benefits and externalities

Renewable energy has been widely embedded in European policy targets to reduce fossil energy dependence and, in addition, to limit greenhouse gas emissions (EU Directive, 2009). Among the different renewable energy resources, wind energy is currently very popular in Europe and has been employed for large-scale electricity generation projects (EWEA, 2015). In addition, the low greenhouse gas footprint and the minimum water demand are making wind energy a popular alternative to fossil fuel in Europe (Deal, 2010; Evans et al., 2009). The *EU climate and energy package* has set the target of 20% for the overall EU energy shares from renewable energy resources by 2020 (2020 Climate and Energy Package, 2009), in which the Netherlands target is 14% (EU Directive, 2009). In line with this policy, the Dutch government intends to expand its on-shore wind energy production by 2020–6000 MW (SER, 2013).

Despite the potential benefits of wind energy, there is an

* Corresponding author. Department of Spatial Economics/SPINlab, VU University Amsterdam, De Boelelaan 1105, 1081 HV Amsterdam, The Netherlands.
E-mail address: a.rafiee@vu.nl (A. Rafiee).

[1] https://github.com/NetTopologySuite/GeoAPI.
[2] https://github.com/GeoJSON-Net/GeoJSON.Net.
[3] http://www.newtonsoft.com/json.
[4] https://dotnetzip.codeplex.com/.
[5] https://proj4net.codeplex.com/.
[6] https://github.com/leonbloy/pngcs.
[7] https://docs.unity3d.com/Manual/UsingDLL.html.
[8] https://www.microsoft.com/nl-nl/download/details.aspx?id=1639.

http://dx.doi.org/10.1016/j.envsoft.2017.06.019
1364-8152/

important debate regarding the wind turbines' externalities, among which noise is perceived as the most critical (Saidur et al., 2011). Studies have explored different impacts of wind turbine noise on human health, among which we find: annoyance, sleep disturbance, psychological distress, headaches, concentration difficulties, tiredness and auditory system problems (Bakker et al., 2012; Pierpont, 2009; Pedersen, 2011). The externalities from wind turbine noise can be severe enough to force people to leave their residences (Arezes et al., 2014) and may lead to a fall in property values in the vicinity of the wind turbine (Saidur et al., 2011). Naturally, the expectation and anticipation of these detriments give rise to resistance among local communities and residents against wind turbine installation in their surroundings.

1.2. Incorporation of an information system into a 3D virtual environment to facilitate discussion

The negative opinion of residents towards wind turbines, due to their noise, can be intensified by the lack of information on the actual consequences of a wind generation project. This amplified negativity may be moderated through access to a validated information system embedded in a collaborative platform that enables discussion and facilitates information-sharing between the local community and the wind energy developers (Groth and Vogt, 2014). Transparent information and the involvement of local communities from the initial phase of the planning process have been reported to restore trust and to influence the social acceptance of projects (Jobert et al., 2007; Hall et al., 2013) and is considered essential for forming long-term solutions that potentially get long-lasting support (Tippett, 2005).

Beyond the information itself, the visualization of the information also influences its understandability and reception (Al-Kodmany, 1999). 3D virtual environments have been used to present information in different planning processes (Stock et al., 2008), including wind turbine planning (Bishop and Stock, 2010; Jallouli and Moreau, 2009). The outcome of these studies highlighted the advantages of the virtual environment in terms of providing instant feedback, more freedom, a more natural user interface and interactivity as significant positive aspects (Bishop and Stock, 2010). Our contribution, compared to the latter study, is the integration of detailed sound models and their real-time numeric presentation, the incorporation of GIS functionalities into the game engine and therefore the independency from third party software packages and embedding web services and open standard protocols, which together with tiling techniques enables the on-the-fly loading of massive geospatial datasets from different sources and eliminates the interoperability problem between them. These are explained later in the article.

1.3. Game engine-based virtual environment for planning processes

The use of computer games and game engines in environmental applications and planning is increasing due to their advanced performance and interactivity capabilities (Herwig and Paar, 2002). If well designed, games enable the inclusion of target groups without expert proficiencies into a multi-disciplinary environment since they provide familiar settings for unfamiliar subjects. This makes games an effective educational tool that facilitates knowledge and information exchange (Bishop, 2011).

A 3D game engine includes numerous key runtime components that enable efficient game development and performance, such as the rendering engine, physics engine, animation modules, collision detection, scripting, visual effects, threading, memory management and math libraries (Gregory, 2009).

Herwig and Paar (2002) concluded, based on a planning workshop, that the landscape visualization offered by the graphics-assisted games triggers public interest in the planning process. In another study, the application of game engines in participatory design processes was investigated and evaluated through a comparison with conventional participatory tools (O'Coill and Doughty, 2004). Different test settings confirmed the participants' enhanced understanding of design problems through the real-time visualization of information via the computer game, which helped the participatory process to a great extent.

Following these efforts, in this paper we present our study on the development of a 3D GIS-integrated virtual environment based on the Unity game engine (Personal version)[9] for supporting wind turbine planning processes with the emphasis on wind turbine noise estimation. This has been carried out via the Unity scripting API [10] through the integration of self-developed functionalities as well as applying the existing libraries (mentioned in Software availability Section).

1.4. Actual objects in the virtual environment: GIS integration

Game engines have great potency as a design platform due to their optimized performance, graphic abilities and adaptable (user-friendly) interface, but their detachment from the GIS environment limits their ability to be used stand-alone in a planning process, since most existing geospatial information and the analytical impact calculation functionalities are usually only available in GIS environments. The integration of GIS in a game engine, wherein geographic coordinate systems and GIS functionalities are managed, is a crucial step, as identified in previous studies (Bishop and Stock, 2010; Herwig and Paar, 2002). In this research, we have integrated GIS within our gaming environment and called this integration Falcon.

1.5. Environmental information integration through "sound propagation-GIS-game engine" incorporation

While visual presentation of geospatial information can influence subjective perceptions of visual impacts of wind turbines, the results of quantitative modelling provide an objective evaluation of direct environmental consequences. Among these different impacts, wind turbine noise is considered as a major externality (Section 1.1). Our developed system offers the possibility for wind turbine sound estimation on the surrounding buildings, through the incorporation of sound propagation models. The benefits of game engine and GIS integration for the sound model implementation lies in the real-time and interactive performance of its modules for the whole country. The incorporation of sound propagation-GIS-Game engine model triplet supported the development of an integrated environmental information system for wind turbine planning where the interactivity, real-time performance and on-the-fly massive geospatial information visualization are its key features.

2. Methodology

2.1. System architecture

Fig. 1 presents the client–server architecture of our developed 3D game engine-based virtual environment as a three-tier configuration. This framework is composed of the visualization/interaction, processing and data tiers, illustrated here as *Unity game engine*, *services* and *database*.

[9] https://store.unity.com/products/unity-personal.
[10] https://docs.unity3d.com/ScriptReference/index.html.

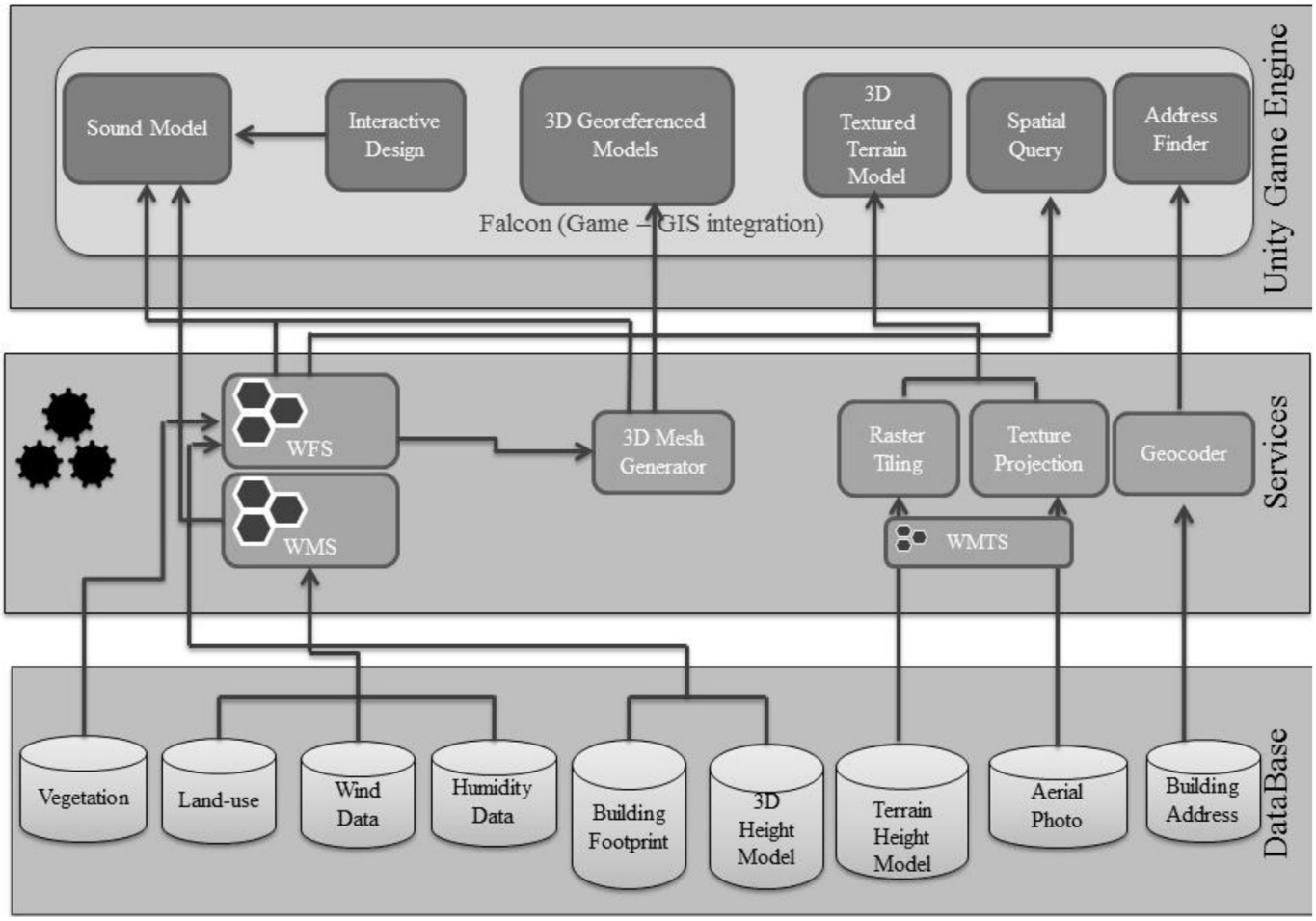

Fig. 1. System architecture.

The data tier consists of different distributed databases comprising the input parameters for the sound model, as well as the data for 3D visualization and the background scene. These georeferenced data are stored in the cloud and are transferred through OGC WMS, WFS and WMTS standard web services. Web services are particularly appropriate for an effective visualization purpose, as a key element in decision support systems (Vitolo et al., 2015).

A 2.5D terrain model of the Netherlands, textured with an aerial photo, is generated using terrain height data and loaded in Falcon. As the terrain model and its aerial photo texture for a large area (in this case, the whole country) are massive, they cannot be served all at once and an efficient technique should be utilized to manage them. Therefore, we have applied raster tiling operations to serve these datasets for the whole country. Raster tiling for the terrain height model and aerial photograph-both with 50 cm spatial resolution-of the whole Netherlands is performed through pre-rendered georeferenced tile generation, for different zoom levels, from the whole raster datasets and served based on the WMTS standard protocol (Masó et al., 2010). Based on the camera position and the zoom level, a request is sent to the server, wherein the predefined tiles are hosted, to get the underlying tiles. Each terrain height tile is RGB color coded and contains 256 × 256 pixels. Each pixel is converted from RGB to height value (in centimeter) through the following transformation:

$$H_t = (256 \times 256 \times R) + (256 \times G) + B \quad (1)$$

Where H_t is the terrain height in centimeters, and R, G and B are the red, green and blue values of the color coded tile pixel, respectively.

For each terrain height tile, a game object mesh is generated and the relevant aerial photo tile is queried, based on its georeferenced coordinates. The aerial photo is projected on the terrain height tile through the Unity game object material *shader* class. The result is a tiled 3D terrain height model, textured with an aerial photo, whose height properties can be queried by different components and can be used in different collision detections.

3D building model generation and vector tiling are performed in Falcon for displaying 3D building models of the whole Netherlands. 3D building models are generated by overlaying the open data of (2D) cadastral building footprints[11] on a 3D LIDAR point cloud dataset[12] based on their georeferenced X and Y coordinates. For each building, a statistical height average is estimated from all the intersecting LIDAR point cloud Z values and assigned to the 2D building footprint as its attribute. 2D building footprints with their assigned height attribute are transferred to the cloud through WFS protocol. Falcon's compatibility with the WFS standard makes it possible to retrieve the buildings geometry and the attributes of a specific boundary on the fly from the cloud data repositories using *GetFeature Request*[13]. Upon camera movement in the game scene,

[11] http://www.kadaster.nl/web/show/id=102363.
[12] http://www.ahn.nl/index.html.
[13] This function is defined by OGC WFS and returns features (geometry data and attributes) of a selected region (Vretanos, 2005).

its georeferenced coordinates as well as the zoom level of the scene are used for the determination of the boundary for which the buildings geometry and attributes are requested through WFS. This data is sent to the *3D Mesh Generator* module in Falcon, where 3D building models, as game objects, are generated through 2D footprint extrusion based on their height attributes. These models are presented in a Falcon game scene as 3D building models.

The geocoder service is an OpenLS service[14] provided by the Dutch National SDI (PDOK[15]) which specifies the coordinates of an address. Embedding this service into Falcon provides the users with quick navigation to a desired address.

The visualization/interaction tier is a 3D platform based on the Unity game engine. It is developed via the C# API of Unity and can be accessed through a web browser or as a mobile/desktop standalone application. Different 2D/3D georeferenced data are retrieved from the web and presented through introducing geospatial coordinate systems and the incorporation of GIS functionalities and data standards in Falcon. Beyond being a geovisualization tool, the Falcon visualization/interaction tier is also a design platform in which 3D or 2D elements can be added (also removed or altered) to the existing world to compose a new landscape scene, which makes it an interactive input–output platform. In this case study, users can add different 3D wind turbine models of various types (available in the Falcon library), scale and rotate them in different axes, change their position and remove them. The users can then see the visual impact of the wind turbine placement and, beyond that, the influence of its sound on the surrounding buildings is calculated in real time and presented both graphically (by colourizing the buildings based on the received dB) and numerically (through numbers regarding the distribution of the received dB on buildings) to the user. This is performed through the integration of the sound models into the game engine-based Falcon platform via the Unity C# API. The implemented wind turbine sound models are described in the following section.

The seamless movement of a wind turbine in the game scene enables the user to explore all desired scenarios rather than a predefined and discrete set of options. This offers more freedom and provides the scope for more creativity and a sense of user-control in scenario formation and alteration. The fast performance of the platform allows for continuous scenario exploration and analysis by the user without interruption (for calculation), which provides an undistracted and immersive experience.

GIS functionalities are integrated in the game engine platform through self-developed C# code which includes self-written functions as well as existing libraries. The existing libraries our code uses are: GeoAPI, Proj4Net and GeoJSON.Net. All the sound models are implemented and integrated in the system through C# code developed by the authors. The game engine, GIS functionalities and sound models interact with each other through the self-developed scripts in Unity C# API. The services tier contains different processes for the processing and serving the data into the visualization/interaction tier. This is carried out through writing new functionalities in C#, which also make use of existing libraries (namely: Newtonsoft.Json and DotNetZip) for applying standard protocols in Falcon. Geospatial datasets (such as land-use) are served as web services published using Geoserver and ArcGIS, but are not limited to these packages, any software capable of serving the data as a standard web service could be used.

[14] [OpenGIS®] Open Location Service.
[15] Publieke Dienstverlening Op de Kaart

2.2. Wind turbine noise

2.2.1. Noise generation

Most recent wind turbine noise models couple aero-elastic wind turbine models, for instance based on the blade-element momentum theory or CFD modelling, to aero-acoustic prediction models based on the Ffowcs-Williams–Hawkings equation (Filios et al., 2007; Oerlemans and Schepers, 2009; Tadamasa and Zangeneh, 2011). Grosveld et al. (1995) presented semi-empirical models for the estimation of inflow-turbulence noise, trailing-edge noise and blunt-trailing-edge noise. The state-of-the-art trailing edge noise model was developed at TNO-TPD in the Netherlands and applied by Moriarty et al. (2005). The application of this model requires the description of aerofoil boundary layer aerodynamics, such as the boundary layer thickness, the friction coefficient and the flow velocity at the edge of the boundary layer.

As an alternative, the aerodynamic noise can be estimated on the basis of a rule-of-thumb model. Manwell et al. (2002) suggested an empirical equation to estimate the noise level L_{WA} as a function of the blade tip speed V_{tip} and the diameter D of the rotor:

$$L_{WA} = 50(\log_{10} V_{tip}) + 10(\log_{10} D) - 4, \tag{2}$$

where L_{WA} is the overall A-weighted sound power level. The L_{WA} according to Equation (2) does not provide the frequency distribution of the sound power level. In addition, Equation (2) expresses the noise source as a point source. Oerlemans et al. (2007) showed that two point sources can be distinguished: one dominant source at the downward moving blade tips and another source at the hub, of which the former mainly results from trailing edge noise and the latter from mechanically generated noise.

With the application of Equation (2), a frequency distribution of the generated sound needs to be assumed, in order to analyse the attenuation of the propagated sound (see Section 2.2.2). To this end, a uniform energy distribution is assumed – with energy content from 500 Hz to 4000 Hz, to which an inverse A-weighting is subsequently applied. This frequency distribution, through which the blade tip speed and the diameter of the particular turbine are expressed, is then used to estimate the propagated sound. To do so, the sound power level is translated into a sound pressure level at unit distance from the sound source first:

$$L_{p_0} = L_W - 10\log_{10}\left(\frac{\rho_{air} c_0 P_{ref}}{4\pi \hat{p}_{ref}^2}\right), \tag{3}$$

in which P_{ref} is the reference power of 10^{-12}W, c_0 is the speed of the sound through the atmosphere, and ρ_{air} the density of the air.

2.2.2. Noise propagation

2.2.2.1. Ray tracing model. For the prediction of the propagation of the noise from a single sound source, ray tracing models are a frequently applied practical basis (Attenborough et al., 1995, 2007; Prospathopoulos and Voutsinas, 2007). These models consider only the propagation of sound in the vertical plane that contains both source and receiver, implying that lateral effects from wind are neglected. Ray tracing models are mainly valid for relatively small wavelengths and are generally applied under assumed homogeneous atmospheric conditions. Given the sound pressure level L_{p_0} at unit distance from a source, the sound pressure L_{p_r} at a receiver location can be obtained from:

$$L_{p_r} = L_{p_0} - \sum A_i, \tag{4}$$

where A_i represents the excess attenuation that may result from geometrical spreading A_{geo}, possible ground reflection A_{ref}, atmospheric turbulence A_{turb}, atmospheric absorption A_{air}, absorption through vegetation A_{veg} and diffraction A_{diff}.

2.2.2.2. Geometrical spreading and reflection. Considering a source at height H and a receiver at B, at a distance L sound waves travel via a direct wave path r_d and a reflected wave path r_r (see Fig. 2). As can be seen, a flat boundary is assumed. The point source, which represents a wind turbine, radiates sound with sound pressure level L_{p_0} at unit distance from the source.

As a result of geometrical spreading, the amplitude of the sound waves decreases. Following the inverse square law, the attenuation from geometrical spreading A_{geo} of a single wave can be found from

$$A_{geo} = 10\log_{10}\left(r_d^2\right), \tag{5}$$

which is defined with respect to the sound level p_0 at unit distance from the source. In the presence of reflected waves, the sound pressure wave p_r at the receiver location can for a given wave number k be expressed in terms of the source wave p_0:

$$\frac{p_r}{p_0} = \frac{e^{ikr_d}}{r_d} + R_p\frac{e^{ikr_r}}{r_r}. \tag{6}$$

This expression, in which $i = \sqrt{-1}$ and which includes the attenuation through geometrical spreading, assumes an acoustically neutral atmosphere, i.e. no refraction, and therefore allows the superposition of the direct and a single reflected wave only (Piercy et al., 1977). R_p is the reflection coefficient of the flat finite impedance boundary. Given the height above the ground of the sound source of a wind turbine, the reflection coefficient R_p can be determined from:

$$R_p = \frac{\sin\theta - Z_{air}/Z_{ground}}{\sin\theta + Z_{air}/Z_{ground}}, \tag{7}$$

where θ is the sound wave incident angle at the ground, $Z_{air} = c_0\rho_{air}$ is the characteristic impedance of air and Z_{ground} the complex impedance of the ground. Empirical formulae for the real and imaginary part of the ground impedance have been derived by Delany and Bazley (1970) through the investigation of the acoustic properties of fibrous absorbent materials. Validation of these relations on the basis of outdoor measurements can be found in Chessell (1977) and Nicolas et al. (1985), while numerical values for the c for a number of ground layer types have been estimated by Embleton et al. (1983) and Attenborough (1992).

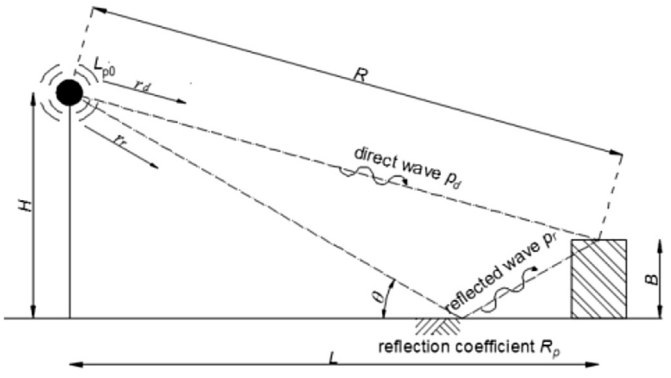

Fig. 2. Graphical representation of the direct and reflected wave.

The interference of direct and reflected sound waves is disturbed by the presence of atmospheric turbulence. The statistical variation, in terms of the long-term average of the mean square of the sound pressure $\langle\hat{p}^2_{r;turb}\rangle$ relative to $\hat{p}_0^2$ can be estimated from (Daigle et al., 1978; Daigle, 1979):

$$\frac{\left\langle\hat{p}^2_{r;turb}\right\rangle}{\hat{p}_0^2} = \frac{2}{r_d r_r}\left\{\frac{\langle a^2\rangle}{2}\left(\frac{r_r}{r_d} + |R_p|^2\frac{r_d}{r_r}\right) + \frac{r_r}{2r_d}\left(1 - |R_p|\frac{r_d}{r_r}\right)^2 + |R_p| + |R_p|\left(1 + \left\langle a^2\right\rangle\rho_a\right)\cos(\phi_r + \gamma)e^{-\left\langle\delta^2\right\rangle(1-\rho_\delta)}\right\}, \tag{8}$$

where γ is the phase angle of the complex reflection coefficient, $R_p = |R_p|e^{i\gamma}$. Equation (8) includes the variance of the zero-mean fluctuations of the sound wave amplitude $\langle a^2\rangle$, where it is assumed that the variance of the direct and reflected waves are equal. The same assumption is applied for $\langle\delta^2\rangle$, which represents the variance of the wave number fluctuation of the direct and reflected waves. ρ_a and ρ_δ are the covariances of both the amplitude and the phase, for which it is assumed that $\rho_a = \rho_\delta = \rho$, which can be obtained from (Attenborough et al., 2007). Daigle (1979) presented an approach to estimate $\langle a^2\rangle$ and $\langle\delta^2\rangle$, employing the fluctuating index of reflexion $\langle\mu^2\rangle$, which expresses the meteorological conditions, and a specific turbulence length scale L_{turb}. Numerical values for $\langle\mu^2\rangle$ and L_{tur} were estimated by Johnson et al., 1987for different weather conditions. The excess attenuation in the presence of turbulence A_{turb}, in addition to the attenuation in non-turbulent circumstances, can be obtained from:

$$A_{turb} = 10\log_{10}\left(\frac{\hat{p}_r^2}{\hat{p}^2_{r;turb}}\right). \tag{9}$$

The presented model may be simplified for a direct or reflected wave only, for instance if a receiver is located in the shadow zone behind an obstruction. In this situation, diffraction should be accounted for (see Section 2.2.2.4).

2.2.2.3. Absorption. The attenuation A_{air} due to atmospheric absorption can be obtained from the integration of the absorption coefficient α over the source–observer length:

$$A_{air} = \int_0^R \alpha\mathrm{d}r \tag{10}$$

A_{air} results from the integration of the frequency-dependent absorption coefficient α along the wave path over the total length from the source to the receiver. The absorption coefficient α can be estimated from the ambient temperature T, relative humidity h and atmospheric pressure (Bass et al., 1990). If direct and reflected waves are considered, the atmospheric absorption can be calculated for both.

Fig. 3 presents a sound wave p travelling over a distance R from a source towards a building. This sound wave crosses a green belt in front of the building. The crossing distance is L_{veg}. Kurze (1971) developed a theoretical model for the attenuation of sound propagation through trees, where the attenuation is only a function of the frequency and the crossing distance:

$$A_{veg} = 0.01L_{veg}\sqrt[3]{f} \tag{11}$$

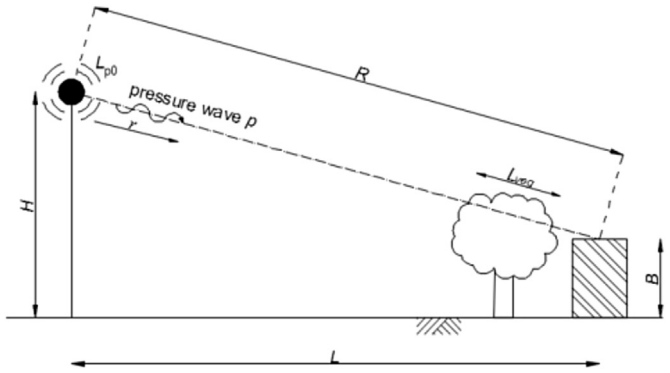

Fig. 3. Graphical representation of the absorption through vegetation.

2.2.2.4. Diffraction. As buildings have very limited transmission of sound waves, the sound level at the back of a building can be assumed to be significantly less than the level in front of the obstruction. Still, as a result of diffraction, sound waves will penetrate into the shadow zone behind the obstruction (see Fig. 4). Kurze and Anderson (1971) developed an engineering model to estimate the sound attenuation due to a rigid infinitely long barrier for sound from a point source:

$$A_{diff} = \begin{cases} 20\log_{10}\left(\dfrac{\sqrt{2\pi N}}{\tanh\sqrt{2\pi N}}\right) + 5, & \text{for } N \geq -0.2 \\ 0, & \text{for } N < -0.2 \end{cases} \quad (12)$$

The Fresnel number N is a measure of the distance of the location of the receiver from the line of sight towards the source, relative to the wavelength λ:

$$N = \pm\frac{2}{\lambda}(R_A + R_B - R) \quad (13)$$

N is positive if the receiver is located in the shadow zone behind the barrier, otherwise N is negative.

The attenuation derived with Equation (12) was found to be conservative in comparison with the experimental results presented by Maekawa (1968). Nevertheless, the approach assumes a semi-infinite barrier and does therefore neglect reflections at the ground behind the barrier. Moreover, diffraction from sound waves travelling along the sides of the barrier are not accounted for. To account for this diffraction along the sides, however, the diffraction model given by Equation (13) could be employed too, with R_A and R_B now defining the indirect sideways wave paths.

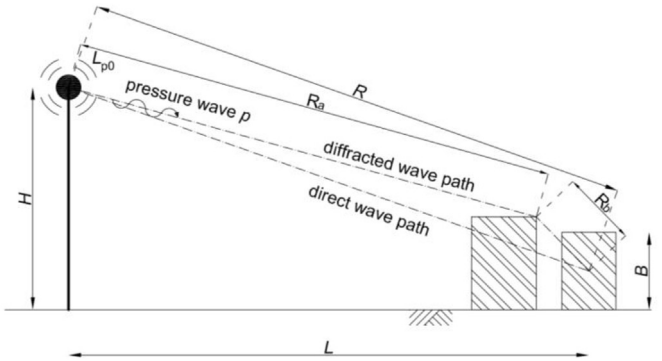

Fig. 4. Graphical representation of the direct and diffracted wave.

2.2.2.5. Refraction. The presented noise propagation models did not account for the presence of wind and a temperature gradient, both of which affect the sound pressure level at the receiver location. Wagner et al. (1996) presented an overview of the effects of weather on the propagation of wind turbine noise. Both wind and temperature gradient affect the sound wave pattern, potentially resulting in sound shadow zones.

The location of the edge of a shadow zone can be estimated on the basis of R_{shadow}, according to the following expression:

$$R_{shadow} = c_0\left(1 + \frac{V}{c_0}\right)^3\left(-\frac{V}{c_0}\frac{\sqrt{\kappa c_g}}{\sqrt{T}}\frac{dT}{dz} + \frac{dV}{dz}\right)^{-1}. \quad (14)$$

This formula contains the wind velocity V and the ambient temperature T, as well as the corresponding gradients with respect to the height z. κ is the adiabatic gas constant, c_g the specific gas constant. The wave propagation velocity through ideal gases can be found from

$$c_0^2 = \kappa c_g T \quad (15)$$

The wind velocity gradient with respect to height can be determined from a reference wind velocity, commonly defined at a height of 10 m – V_{10}:

$$\frac{dV}{dz} = \frac{V_{10}}{z\ln(10/z_0)}, \quad (16)$$

making use of the roughness height z_0. Fig. 5 illustrates the shadow zone on the basis of R_{shadow}. Whether a building with a height B is completely located within the shadow zone can be checked on the basis of the following inequality:

$$L \geq \sqrt{R_{shadow}^2 - (R_{shadow} - H)^2} + \sqrt{R_{shadow}^2 - (R_{shadow} - B)^2} \quad (17)$$

3. Framework implementation

The developed framework design is implemented through Unity scripting API.

In addition to 3D building models, users can load raw LIDAR point clouds in Falcon for more detailed interpretation and analysis. Fig. 6 presents AHN2 LIDAR point clouds overlaid on 3D building models in Falcon.

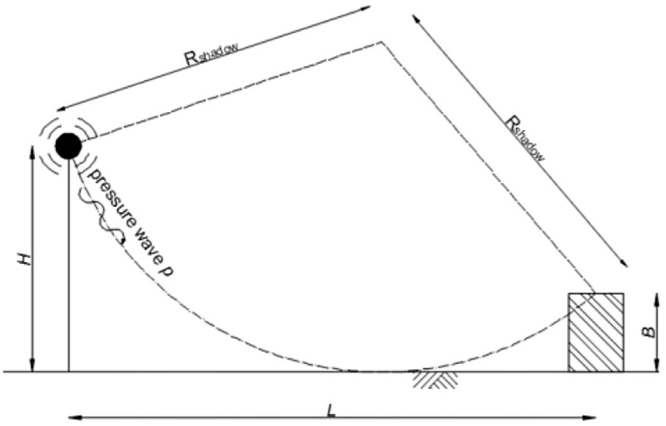

Fig. 5. Graphical representation of the shadow zone resulting from the curvature of the sound waves.

Fig. 6. AHN2 LIDAR point cloud overlaid on 3D models in Falcon. Different 3D and 2D geospatial data of the whole Netherlands are served to Falcon via web services.

Falcon delivers an extensive library of 3D models of different wind turbine suppliers which are available directly from the interface. For each wind turbine, its geometric and technical specifications, such as hub height, rotor diameter, blade tip speed and rated power are stored in the Falcon database and used both for wind turbine information presentation and also subsequently in the sound models. Fig. 7 presents the wind turbine scenario forming in the design environment of Falcon. Users can select a specific wind turbine from the list and add it to the scene. Technical information on the added wind turbine is presented in a separate window.

Each module of the sound model (e.g. diffraction, ground interference) can be accessed and visualized separately in Falcon. Integration of these sub-modules in the game engine-based Falcon helps the user to gain insight into the wind turbine noise behaviour and offers noise experts an interactive fast-performing platform to carry out various types of analysis on the constituents of wind turbine noise. Table 1 presents the implementation architecture of the sound propagation sub-modules. The applied technique types and domains as well as the deployed datasets are described in this table.

Incorporation of the different techniques from the game engine and GIS domains, resulting from the game engine–GIS integration, supports the efficient implementation of the sound sub-modules in an allied environment. While the mutual benefits of game engine and GIS are described in the previous sections, we have performed tests to measure the 3D distance and 3D collision detection performance (in time) with and without game engine-GIS integration. In the first test, 3D distance performance is measured for 2600 buildings in Falcon, with game engine-GIS integration and subsequently, for the same buildings, 3D distance is measured in a pure GIS environment (ArcGIS 10.2.2). The test results indicate that it takes 4 ms for Falcon (game engine-GIS integration) to calculate versus 1.90 s in ArcGIS for the 3D distance functionality. In the second test, 3D collision detection performance was tested for the same buildings as the previous test set. These tests indicated that it takes 20 ms for Falcon (game engine-GIS integration) to calculate versus 1 min and 47 s in ArcGIS for 3D collision detection performance. In both tests, the game engine-GIS integration and the pure GIS environment return the same results and the difference is the performance duration.

The ultimate sound impact of a wind turbine is calculated using the total sound model, composed of all the individual modules. The implementation of each individual sound module is presented as follows.

3.1. Noise generation

Upon adding a wind turbine to the scene, wind turbine characteristics are retrieved from the database and applied in the turbine's overall A-weighted sound pressure level calculation (Equation (3)). This value is presented together with other specifications of a selected wind turbine (Fig. 7).

3.2. Geometrical spreading

Upon the placement of a wind turbine in the scene, the information on all the buildings within 1 km of the turbine is queried. Subsequently, the distance from the turbine to each of these buildings is calculated and the geometrical sound attenuation is computed for the building. The input parameters for this sub-module are the wind turbine geometrical properties as well as the location and height of the surrounding buildings. The sound attenuation values will change in real time when the user moves the wind turbine in the scene. The attenuation distribution is demonstrated numerically (top right) and graphically through colourized buildings and the similarly colourized chart (top middle). The fast responsiveness of the geometrical attenuation module upon the turbine's movement is illustrated in Film 1.

Supplementary video related to this article can be found at

Fig. 7. Wind turbine scenario design in Falcon. Users can select different wind turbine types and bring them into the scene as game objects. By placing a wind turbine in the scene, its geometric and technical characteristics are retrieved from the database and are presented.

http://dx.doi.org/10.1016/j.envsoft.2017.06.019.

3.3. Diffraction

With the existence of an obstacle between the sound source and the receiver, sound waves diffract around the obstacle to move towards the receiver. This leads to a reduction in the sound level.

For each building, a line of sight is defined from its 3D centre point to the wind turbine hub location. The collision between this line of sight and other buildings is examined by the line casting and collision detection features of the game engine. For detecting a collision between the line of sight and another building, the 3D distances between the receiver–obstacle, the target building–obstacle and the receiver–target are calculated using the collision coordinates information. These 3D distances are applied in the calculation of the Fresnel number (Equation (13)) to estimate the sound attenuation due to the collided building (Equation (12)).

In a GIS system, obstacle detection is commonly performed through the 3D visibility analysis method. This approach is computationally demanding, reducing the performance and limiting its usability for real-time operations. However, the real-time collision detection of the game engine, through its physics engine's physical simulations, greatly increases the efficiency of the real-time diffraction calculation. Film 2 illustrates the real-time calculation/feedback of the obstruction attenuation module. The sound attenuations on the lower buildings whose lines of sight are obstructed by taller buildings are more intense.

Supplementary video related to this article can be found at http://dx.doi.org/10.1016/j.envsoft.2017.06.019.

3.4. Ground interaction

The sound level attenuation due to ground reflection on the exposed buildings (buildings without any obstacles to the wind turbine) is calculated based on Equation (8). The input data for this calculation is the land-use map of the Netherlands, the 3D building and wind turbine models and the wind data (derived from the Royal Netherlands Meteorological Institute (KNMI[16]) mean hourly dataset) which is used for the estimation of the reflection fluctuating index. The land-use map of the Netherlands with the scale of 1:10000 is published by the Dutch Central Bureau of Statistics[17]. This dataset is loaded in Falcon through the WMS standard and the

[16] Koninklijk Nederlands Meteorologisch Instituut

[17] Centraal Bureau voor de Statistiek (CBS) (http://www.cbs.nl/nl-NL/menu/home/default.htm).

Table 1
The applied techniques and data for each sound sub-module.

Sound Module	Technique		Data
	type	domain	
Geometrical Spreading	3D Distance	Game engine	3D building models Wind turbine characteristics
Atmospheric Absorption	GetFeatureInfo Request[a]	GIS	Temperature Humidity
	3D Distance	Game engine	3D building models
Vegetation Absorption	3D Line Casting	Game engine	Land-use
	3D Distance	Game engine	Wind turbine characteristics
	GetFeature Request	GIS	3D building models
Ground Interaction	3D Distance	Game engine	Land-use Wind turbine characteristics
	GetFeatureInfo Request		3D building models
	GIS		Wind
Obstruction/ Diffraction	3D Distance	Game engine	Wind turbine characteristics
	3D Line casting 3D Collision Detection	Game engine	3D building models
Weather Effects/ Refraction	3D Distance	Game engine	Wind Temperature
	GetFeatureInfo Request	GIS	3D building models

[a] This request is defined by the OGC WMS implementation and it retrieves the location and attribute information of a pixel in a specific location of a map (de La Beaujardière, 2002).

raster tiling technique.

For each receiver (i.e. building), the sound wave incidence angle at the ground is calculated using the wind turbine and building coordinates. This angle is used in combination with the impedance characteristics of air and the complex impedance of the ground for the calculation of the ground reflection coefficient (Equation (7)). Real and imaginary parts of the complex impedance of the ground are a function of the flow resistivity of the surface and sound wave frequency. Flow resistivity determines the ease of air movement in and out of the surface and is inversely proportional to porosity (Crocker, 2007). In the case of surfaces of constant porosity, the flow resistivity of the surfaces can be assigned with a single value (Piercy et al., 1977). Table 2 presents the flow resistivity values used in this research (Piercy et al., 1977; Forrest, 1994).

When a wind turbine is placed on the ground, the land-use type of the location will be queried from the land-use map, through the WMS "*GetFeatureInfo Request*", which will be used to estimate the flow resistivity value. The flow resistivity of the surface, together with the position/height of the wind turbine and the building, are used in the calculation of the reflected sound wave. Fig. 8 presents the impact of different land-use types on the receiving noise of each exposed building. We assumed the resistivity of arable land in the range of grass, rough pasture, being 250 cgs rayls.

Table 2
Flow resistivity values for different surface types.

Surface	Flow resistivity (cgs rayls)
In forest, pine or hemlock	20–80
Grass, rough pasture	150–300
Roadside dirt, ill-defined, small rocks up to 10 cm diameter	300–800
Sandy silt, hard packed	800–2500
Clean limestone chips, thick layer (12–25 mm mesh)	1500–4000
Earth, exposed and rain-packed	4000–8000
Water	10000
Quarry dust, fine, very hard-packed by vehicles	5000–20000
Asphalt, sealed by dust and use	>20000

3.5. Effect of vegetation

Dense enough vegetation can lead to sound attenuation if it blocks the view between the sound source and the receiver (Section 2.2.2.3). To distinguish densely vegetated areas from sparse ones, we have extracted the forest regions from the vector land-use map of the Netherlands. The average height of the forested region is estimated using the DSM[18] of the area (derived from the LIDAR point cloud) and assigned to each vector feature. The forest vectors are loaded in Falcon and their geometries and attributes are retrieved through the WFS "*GetFeature*" request. Upon the placement of a wind turbine in the vicinity of a forest, a 3D line-of-sight analysis is performed for each building to detect its visibility status from the wind turbine through the forested area. If the line of sight between a building and the wind turbine is blocked by the forest (considering its height), the sound attenuation on the building due to the forest is calculated using Equation (11). The vegetation length between the wind turbine and each building is estimated through the retrieved forest vector geometries and the building location. For this estimation, two forest polygon vertices, namely the nearest vertex to the wind turbine and the nearest vertex to the building, are queried and applied in the Euclidian distance calculation.

Fig. 9 presents the sound attenuation due to vegetation absorption. The AHN2 LIDAR point cloud of the area has been loaded in Falcon to present the 3D morphology of the forested region. The attenuation is different for buildings with different heights and different distances to the wind turbine. To present this geometrical relation, two scenarios have been depicted in Fig. 9. In each scenario the wind turbine is sited at a different location and distance relative to the target buildings. As the wind turbine moves further from scenario *a* to *b*, the lines of sight between the wind turbine and more buildings are blocked by the forest and therefore the number of buildings affected by vegetation absorption increases.

The input data of the vegetation sub-module comprises the wind turbine data, the vector land-use data and the 3D building models. 3D distance and line casting operations are the game engine techniques used in this sub-module.

3.6. Effect of atmospheric absorption

Upon the placement of a wind turbine on a location, the temperature and humidity values of the site (obtained from the KNMI hourly open data) are queried and employed in the atmospheric absorption sub-module.

Alternatively, the user can define the temperature and humidity of each location manually using the sliders provided in the Falcon interface. This offers the possibility of comparative studies (e.g. on different seasons or extreme case scenario assessments), where different temperature and humidity values lead to different atmospheric absorption attenuation and the final wind turbine sound effects. Fig. 10 presents the implementation of atmospheric absorption attenuation in the Falcon interface under two different humidity conditions. Fig. 10a presents the atmospheric absorption for the current humidity situation of the study area. As mentioned above, the humidity of a location is estimated based on the KNMI

[18] Digital Surface Model.

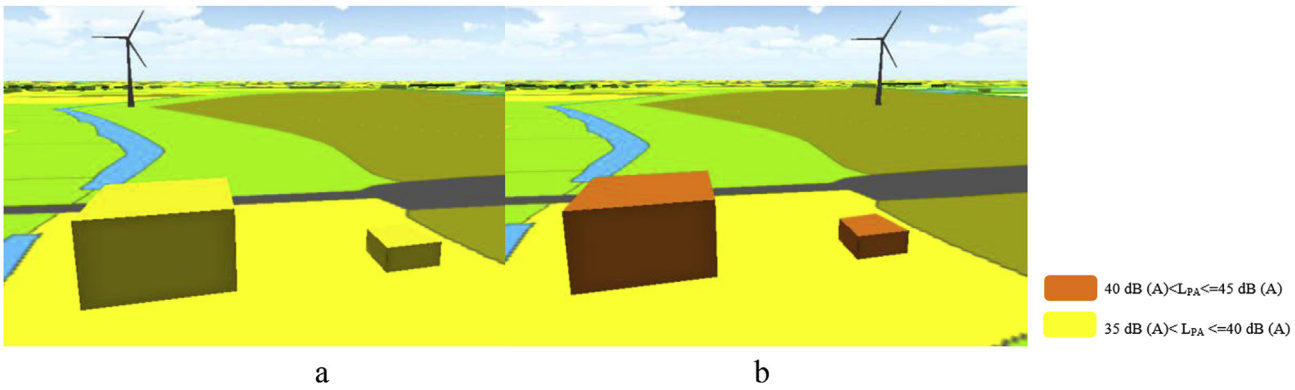

Fig. 8. Placement of the wind turbine on different land-use types leads to different noise being received on the same buildings: a) grass field and b) arable land. All other parameters (e.g. wind turbine-building distance) remain the same.

hourly data, which is 80.6% for this location. Fig. 10b shows the humidity adjustment possibility in Falcon and its influence on the atmospheric absorption results. In this case, the humidity is set as 20%. It can be seen that in the lower humidity condition, the atmospheric absorption is higher. This leads to a lower sound level being received at the surrounding buildings. The real-time calculation/feedback of the atmospheric absorption module upon the wind turbine's movement and humidity alteration is illustrated in Film 3.

Supplementary video related to this article can be found at http://dx.doi.org/10.1016/j.envsoft.2017.06.019.

3.7. Effect of wind

As mentioned in Section 2.2.2.5, at specific distances and directions, the sound pressure level declines suddenly, forming so-called “shadow zones”, where direct sound rays cannot penetrate. We have calculated the radius of the shadow zone based on

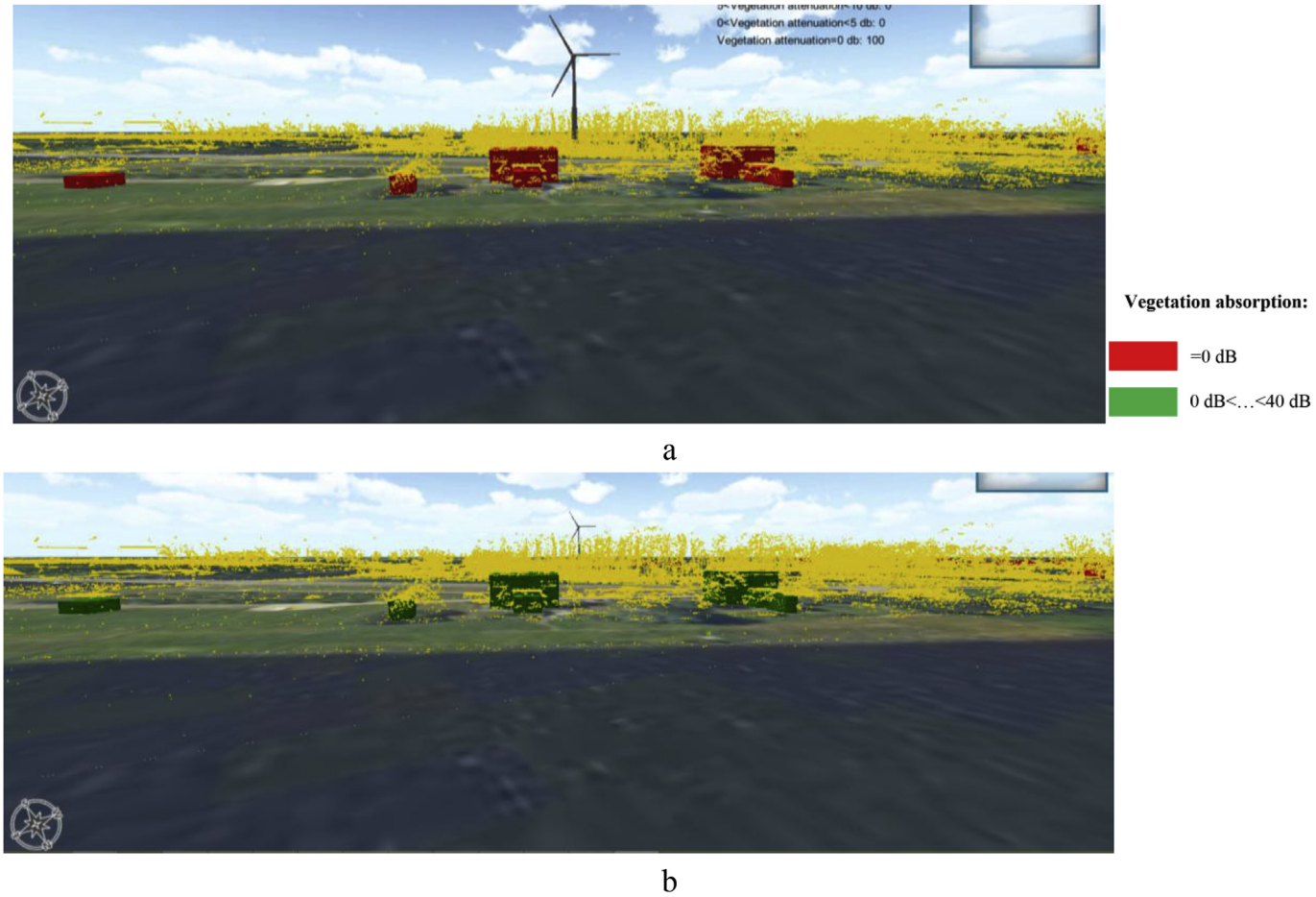

Fig. 9. Sound attenuation due to vegetation (sound frequency is set to 1000 HZ) depicted in two scenarios. By placing the wind turbine further from the target buildings from scenario *a* to *b* the number of buildings affected by line-of-sight obstruction by the forest increases.

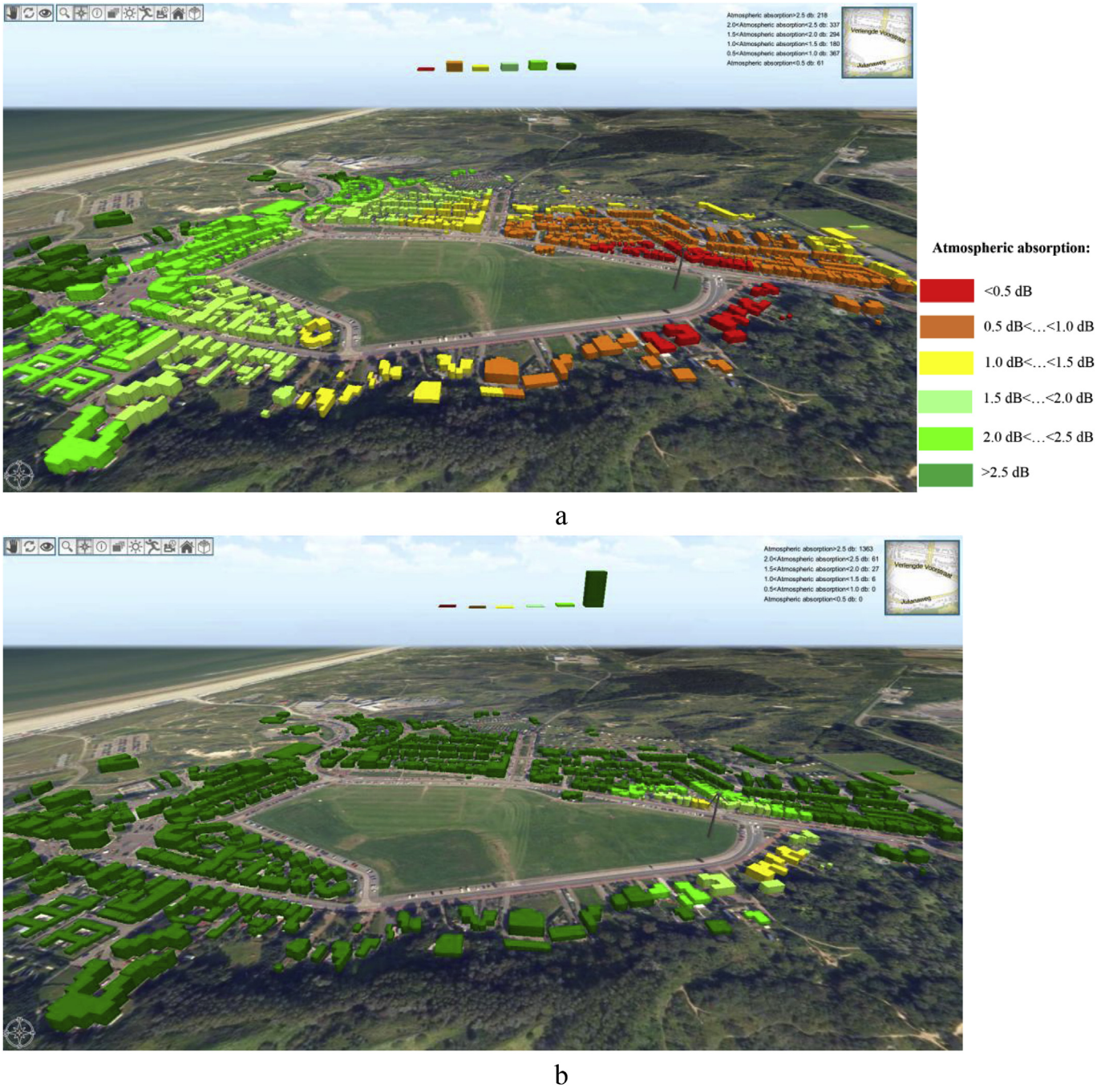

Fig. 10. Implementation of atmospheric absorption sub-module for a) current humidity situation estimated by hourly humidity data (80.6%) and b) adjusted humidity (20%).

Equation (14).

By placing a wind turbine in the scene, the wind properties of the location vicinity are extracted from the mean hourly wind data provided by KNMI to calculate the radius of the shadow zone. The direction of the shadow zone is defined according to the dominant (or actual) wind direction of the region.

Once the shadow zone radius and the direction are calculated for the specific location of the wind turbine, based on the location and height of each building and the turbine, it can be checked whether it falls within the shadow zone or not (Equation (17)). Unlike all the other sub-modules in which the calculations are performed for the buildings within 1 km of the wind turbine, the computations of this sub-module are implemented for buildings within 3 km of the wind turbine. This is due to the greater distances where weather effects have an impact.

The mean hourly wind data, the wind turbine data and the 3D building models are the underlying data for the wind sub-module (see Table 1). The real-time calculation/feedback of the wind effect module is illustrated in Film 4. This film presents the buildings falling within the wind shadow zone (in black) into which no direct sound ray can enter. These buildings are located approximately 1.6 km from the wind turbine.

Supplementary video related to this article can be found at http://dx.doi.org/10.1016/j.envsoft.2017.06.019.

4. Results

The performance of our developed system and the underlying sound model are analysed for different urban configurations and different climatic situations using the nationwide data accessed via Falcon.

Users can access the tool via an internet browser and have at their disposal different datasets of the whole Netherlands. They can be "teleported" to a specific location by typing its address or navigate to any location through the pan, rotate and zoom functionalities (Fig. 11). The first upper left button in the toolbar is the pan button, the second button is the free rotation and the third one is the rotation from a fixed observer point. Zooming in/out is performed through mouse scroll, zoom in/out buttons in the interface, or pinch in touch interface.

3D models of different wind turbines can be added to the scene as explained in Fig. 7. Upon the placement of a wind turbine in the scene, its location, geometrical and technical information are retrieved and dispatched to all the sub-modules. For the ease of use, only the total sound module is exposed to users by default. The other sound sub-modules can be added by the users for a more detailed analysis (Fig. 12).

4.1. Test cases

The Falcon environment provides the scope for an enhanced insight into the noise from wind turbines in a real-world-related virtual environment. The instant feedbacks, provided through real-time sound model calculations, enable the user to uninterruptedly explore various scenarios of turbine positioning. To illustrate both the performance and the usability of the software, we have performed a number of test cases with different environmental settings and turbine specifications. The visual and numeric outcomes of these test cases are then discussed and compared. Table 3 presents the numeric configuration of each test case. The game interface client application, performing the analysis, is accessed using an Intel Core i7-4790 CPU with an NVIDIA GeoForce GTX 970 graphics card.

4.1.1. Test case 1

The potential for wind energy is greater off-shore than on-shore, due to the undisturbed sea surface, which allows for the development of a stable wind field with greater velocities at smaller heights. Near-shore locations require less expensive foundations than off-shore sites. Moreover, the costs of installation, maintenance and decommissioning are generally lower. Yet, only a limited number of near-shore sites are employed for the exploitation of wind farms, mainly because of the visual disturbance of the environment.

In this test case, the near-shore wind turbine noise propagation on the surrounding buildings is explored. The study area is Urk, a town in the central part of the Netherlands, adjacent to the IJsselmeer. This town is located within the *Noordoostpolder* wind farm, the largest wind park in the Netherlands to date. The wind turbines are placed within 1.5 km of the town, and are therefore influential on the built area. The farm contains both on-shore and near-shore sections, for which, respectively, Enercon E−126 and Siemens SWT-3.0-108 wind turbines are installed.

Fig. 13 visualizes the simulation of the wind turbine noise propagation on the buildings within 1 km distance. Selecting this distance was due to the very low sound level at the further buildings, mainly due to geometrical attenuation. However, this radius can be adjusted differently for different applications. In this simulation a wind turbine with 76 m height and 48 m blade length with nearly 800 kW rated power capacity and 119 dB (A) noise level is chosen. This wind turbine is located in the IJsselmeer, in the vicinity of the built area. This location was chosen to illustrate the working of the sound radiation tool, rather than to represent the positioning of an actual wind turbine. The temperature is set to 15 °C and the wind speed and the humidity, derived from KNMI hourly data, are 4 m/s and 80%, respectively. As seen in the figure, the distance between the buildings and the wind turbine is the main deriving factor in the noise received from the turbine. However, the impact of obstruction can be clearly seen on the lower buildings behind the higher ones. The noise distribution is depicted visually, through colourized buildings and the chart, and numerically on the top right of the UI. The measured total sound calculation time is around

Fig. 11. The user can query a specific location by typing its address or navigate to different locations through pan, zoom and rotate buttons.

Fig. 12. The tool allows the separate implementation of each sound sub-module, as well as the total sound.

Table 3
Numeric configuration of test cases.

Settings		Test Case 1		Test Case 2		Test Case 3		Test Case 4	
Wind turbine	Height (m)	76		45		76		76	
	Blade length (m)	48		44		48		48	
	Overall SPL (dB (A))	119		118		119		119	
Urban Environment	Building height (m)	min	2	min	2	min	2	min	2
		max	15	max	15	max	37	max	37
		mean	6	mean	6	mean	5	mean	5
Climate	Temperature (°C)	15		15		15		15	
	Wind Speed (m/s)	4		4		4		4	
	Dominant wind	West–East		West–East		West–East		West–East	
	Humidity (%)	80%		80%		80%		40%	
Distance	Building–Wind Turbine (m)	min	103	min	76	min	122	min	122
		max	849	max	837	max	981	max	982
		mean	472	mean	458	mean	595	mean	597

600 ms for this test case.

Within the focus area, the majority of buildings (754) receive less than 25 dB (A) noise from the wind turbine, while there are 15 buildings which receive more than 45 dB (A). These distribution results are presented in Table 4.

4.1.2. Test case 2

The turbine characteristics are one of the influential factors on the generation and propagation of wind turbine noise. The hub height, rotor length, drive train and rotational speed are examples of such characteristics. Therefore, different wind turbines in the same landscape settings and climatic conditions induce a different noise distribution.

This test case examines the impact of the characteristics of a wind turbine on the distribution of the noise; the location, urban configuration and climatic conditions are kept the same as in Test Case 1. Here, however, a hub height of 45 m and a blade length of 44 m is selected from the wind turbine list in the Falcon UI. The selected turbine has nearly 900 kW rated power and its sound level is 118 dB (A), which is approximately the same as the sound level of Test Case 1. Fig. 14 presents the noise received at the surrounding buildings.

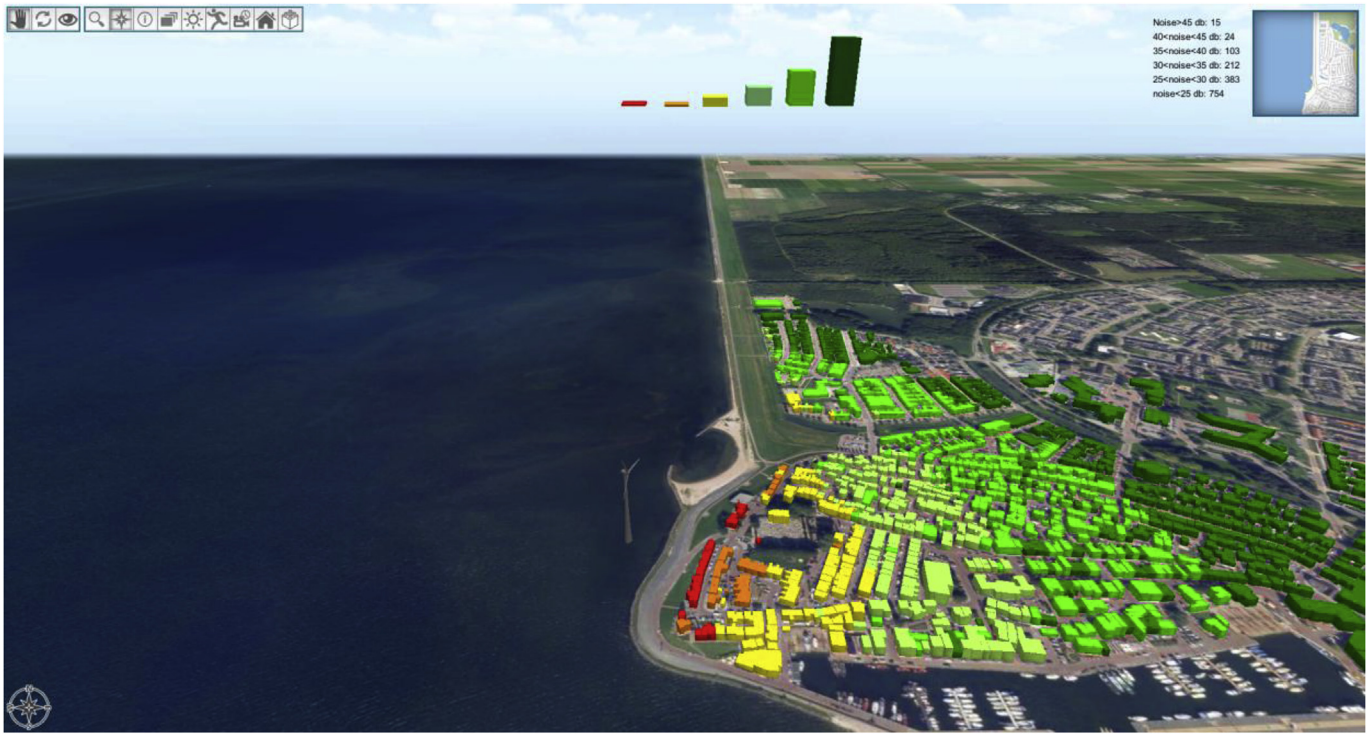

Fig. 13. Wind turbine noise propagation in Test Case 1.

Table 4
Noise distribution in Test Case 1.

Noise level (dB (A))	Number of buildings affected
L_{pA} <25	754
25< L_{pA}<30	383
30< L_{pA} <35	212
35< L_{pA} <40	103
40< L_{pA} <45	24
L_{pA} >45	15

While for high noise levels (nearby buildings) the number of buildings remains comparable to Test Case 1, for the more distant buildings, the number which receive a lower sound level (<25 dB(A)) increases compared to Test Case 1. This is due to the different wind turbine–building line-of-sight geometrical configuration. In the case of a lower wind turbine (this test case) there are more buildings whose lines of sight are obscured by the higher surrounding buildings than in Test Case 1 with the higher wind turbine and therefore experience greater obstruction attenuation. Table 5 presents the number of buildings affected by different sound levels.

Fig. 15 compares the results of the similarly-situated Test Cases 1 and 2. In this figure the percentage of buildings within each noise level is illustrated for each test case.

4.1.3. Test case 3

The vast majority of the wind turbines in the Netherlands are positioned on-shore. Moreover, based on the 2020 target, the on-shore wind power production will increase during the coming years. This test case explores the noise propagation of an on-shore wind turbine towards the neighbouring buildings in an urban area. The study area for this test case is an area in Haarlem. This city is located in the province of Noord-Holland, in the northwest of the Netherlands, where 685.5 MW of on-shore wind energy by 2020 is targeted. A wind turbine with a hub height of 76 m, blade length of 48 m, and 119 dB (A) sound level (the same as Test Case 1) is selected and placed in an agricultural area in the vicinity of the urban area. Fig. 16 presents the sound simulation of the wind turbine noise distribution in this landscape configuration and the same climatic conditions as Test Cases 1 and 2.

The different urban configuration of this test case compared to Test Case 1 leads to a different noise propagation pattern. The tall buildings in this area block the lines of sight of a large number of buildings, which results in higher sound attenuation due to obstruction. The distribution of the number of buildings experiencing different noise levels is presented in Table 6.

4.1.4. Test case 4

The propagation of sound is affected by the climatic conditions. As the meteorological parameters are temporally dynamic, the sound distribution from a turbine alters annually, daily and even hourly. In this case, the impact of alteration of the humidity on the wind turbine sound distribution is illustrated. To perform this analysis, the configurations of the wind turbine and the landscape remain unchanged with respect to Test Case 3. Only the humidity parameter is set differently. While in the other three test cases, the humidity is derived from the hourly mean humidity observation dataset of KNMI, in this test case the humidity is defined manually through the *humidity slider* in the Falcon UI. In this case, the humidity is set to 40%. The wind turbine noise simulation with the adjusted humidity parameter is illustrated in Fig. 17.

Comparing the results with Test Case 3, slight changes in the noise distribution can be observed due to altering the humidity from 80% (Test Case 3) to 40% (Test Case 4). In this test case, more buildings receive a noise level below 25 dB compared to Test Case 3. This is the result of sound attenuation due to atmospheric

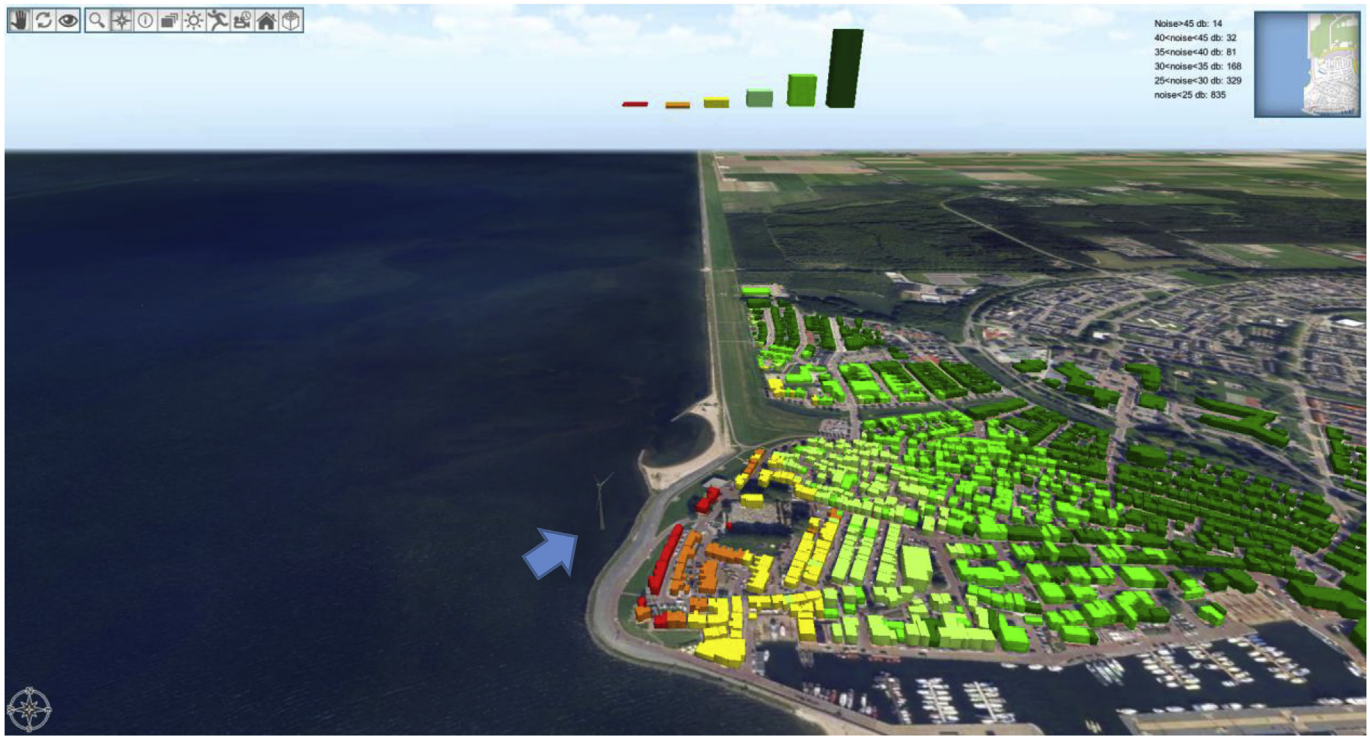

Fig. 14. Wind turbine noise propagation in Test Case 2.

Table 5
Noise distribution in Test Case 2.

Noise level (dB (A))	Number of buildings affected
L_{pA} <25	835
25< L_{pA}<30	329
30< L_{pA} <35	168
35< L_{pA} <40	81
40< L_{pA} <45	32
L_{pA} >45	14

absorption, as discussed in Section 2.2.2.3. This change occurs mainly for the buildings at relatively great distances from the wind turbine (Equation (10)). The numeric distribution of this test case is presented in Table 7.

The comparative sound propagation results of Test Case 3 and Test Case 4 are presented in Fig. 18.

5. Conclusion

This study describes the conceptual design and implementation of an integrated environmental information system for the support of the wind turbine planning process. The developed system is an integration of three major components, namely game engine, GIS and sound model. The easy-to-use interface of the platform allows

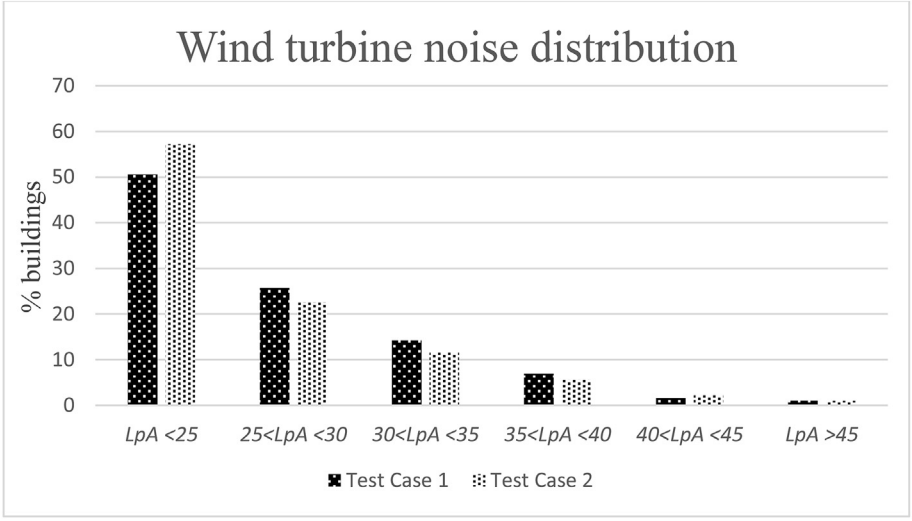

Fig. 15. Comparative results between Test Cases 1 and 2.

Fig. 16. Wind turbine noise propagation in Test Case 3.

Table 6
Noise distribution in Test Case 3.

Noise level (dB (A))	Number of buildings affected
L_{pA} <25	2178
25< L_{pA}<30	510
30< L_{pA} <35	380
35< L_{pA} <40	223
40< L_{pA} <45	21
L_{pA} >45	23

for the contribution of users with different technical backgrounds, and its interactivity, provided through the game engine, has the potential to attract a broader age range, including the very young citizens, who are often absent from the planning process. This transparency of the interaction is considered as one of the most important requirements of a support tool (Geertman and Stillwell, 2012).

Various geospatial data are presented through this platform to the participants, who can interactively build and explore various plan scenarios, in any location in the Netherlands, and see their design impact in real time. Massive geospatial data are served from the cloud and incorporated through the integration of GIS tiling techniques and OGC standard protocols into the game engine via the Unity API. The cloud-based architecture of the framework eliminates the need for local storage and the embedded standard protocols for the data transfer through the web make this platform compatible for accessing and loading various available open data through the internet. This broadens the data accessibility and interoperability and the latter (i.e. interoperability) eliminates the need for data preparation, which leads to considerable efficiency, as in many projects a great amount of time and energy is spent on data preparation and formatting. This is of great importance for a system with several components and inter-related modules, where different data types from different domains and providers must be integrated and be able to interoperate. This can also help the further development of the software by providing the basis for an evolving Spatial Data Infrastructure (SDI) and eliminating the requirement for a whole new geospatial framework construction (Strobl, 2006). Standardization supports the loose coupling of services and their reuse in different software systems (Goodall et al., 2011).

The developed framework provides the possibilities of assessing the aesthetic impact of the wind turbine on the landscape as well as evaluating its noise impact on the surrounding buildings. The aesthetic evaluation is performed subjectively through the 3D model of the existing geospatial data and the 3D wind turbine model. The impact of the wind turbine sound on the surrounding buildings is assessed through sound propagation models integrated into our developed framework and is displayed both numerically and through color variation. The integration of the sound model provides the users with a more accurate estimation and makes the framework appealing for different domains, such as noise experts and legislation authorities. The system provides real-time sound calculations and feedbacks for each design scenario to intertwine the discussion process. We have accomplished this through the game operations as well as the GIS functionalities integrated in Falcon.

While the real-time sound calculations can offer great benefits in a discussion process, it should be noted that some simplifications have been carried out on the sound models for their adaptation to the performance speed. The estimation simplification for combining the direct and reflected waves as well as the modelling of the wave reflection between buildings can be mentioned here. Improving the accuracy of the sound model with the cost of a longer calculation time, would first require a further development of the sound models themselves, an aspect that is not within the scope of this research.

The integration of all the aforementioned separate components into one environment results in a fortified platform with no

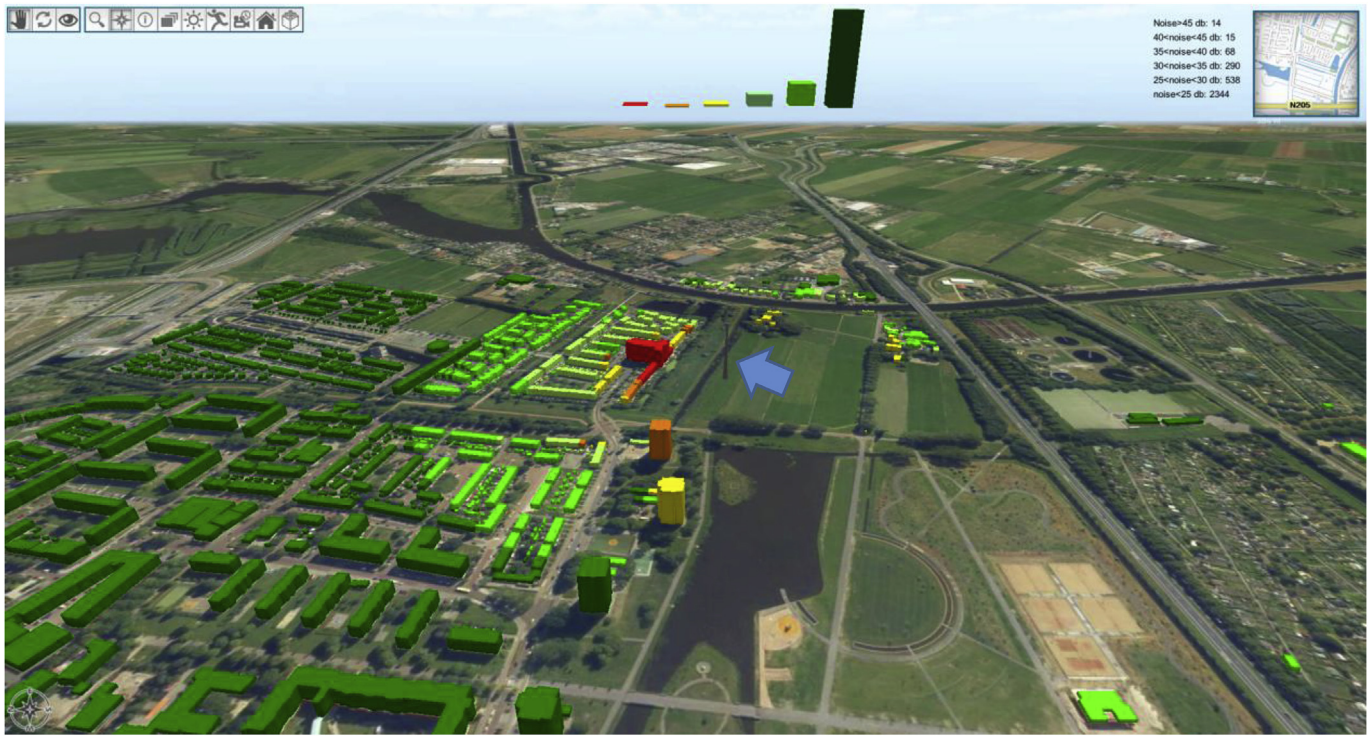

Fig. 17. Wind turbine noise propagation in Test Case 4.

Table 7
Noise distribution in Test Case 4.

Noise level (dB (A))	Number of buildings affected
L_{pA} <25	2344
25< L_{pA}<30	538
30< L_{pA} <35	290
35< L_{pA} <40	68
40< L_{pA} <45	15
L_{pA} >45	14

dependencies on external analytical software. This untangles the game engine disintegration from GIS analytical tools, mentioned by Bishop and Stock (2010) as the limitation of game engines (Bishop and Stock, 2010).

While this platform is presented for the case of a single wind turbine in this study, due to the emphasis on the explanations of the underlying sound propagation models, simultaneous analysis of multiple wind turbines is also possible. This supports the wind turbine scenario formation in larger scales (e.g. wind farms) where the target energy is aimed to be yielded through multiple wind turbines (of different types). This innovative new platform has the potential to make a great contribution to planning processes. However, to evaluate the different benefits and the potential of this framework in a planning process, analysis of the usability and effectiveness should be performed. Further enhancement of this

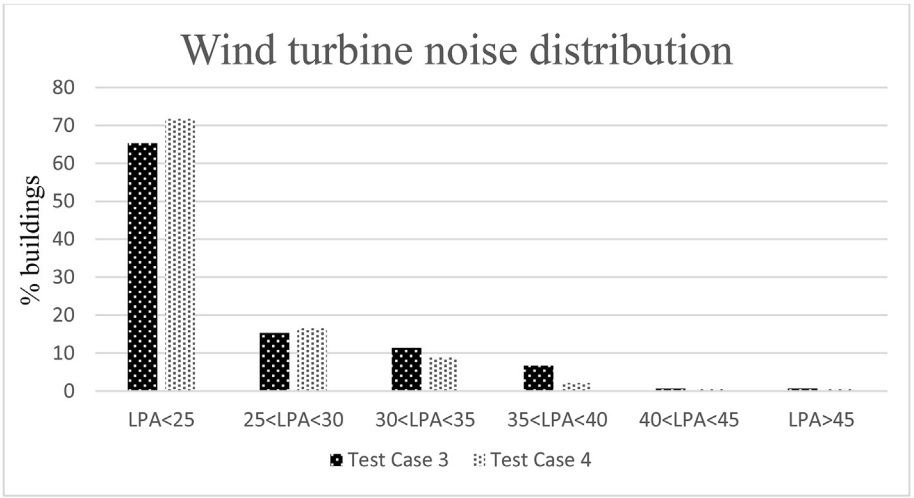

Fig. 18. Comparative results between Test Cases 3 and 4.

framework can embrace other wind turbine externalities, such as shadow effects, as well as wind turbine energy yield models.

Acknowledgements

The authors would like to thank Tim Ebben and Nils Citoleux, the Falcon initiators at Geodan. Special thanks to Steven Fruijtier, the director of Geodan Research Department, for all his supports for this research and his valuable advice and comments on the architecture of the system.

References

Al-Kodmany, K., 1999. Using visualization techniques for enhancing public participation in planning and design: process, implementation, and evaluation. Landsc. Urban Plan. 45 (1), 37–45.
Arezes, P.M., Bernardo, C.A., Ribeiro, E., Dias, H., 2014. Implications of wind power generation: exposure to wind turbine noise. Procedia-Social Behav. Sci. 109, 390–395.
Attenborough, K., 1992. Ground parameter information for propagation modeling. J. Acoust. Soc. Am. 92, 418–427.
Attenborough, K., Taherzadeh, S., Bass, H.E., Di, X., Raspet, R., Becker, G.R., Güdesen, A., Chrestman, A., Daigle, G.A., L'Espérance, A., Gabillet, Y., Gilbert, K.E., Li, Y.L., White, M.J., Naz, P., Noble, J.M., Van Hoof, H.A.J.M., 1995. Benchmark cases for outdoor sound propagation models. J. Acoust. Soc. Am. 97, 173–191.
Attenborough, K., Li, K.M., Horoshenkov, K., 2007. Predicting Outdoor Sound. CRC Press, New York.
Bakker, R.H., Pedersen, E., van den Berg, G.P., Stewart, R.E., Lok, W., Bouma, J., 2012. Impact of wind turbine sound on annoyance, self-reported sleep disturbance and psychological distress. Sci. Total Environ. 425, 42–51.
Bass, H., Sutherland, L., Zuckerwar, A., 1990. Atmospheric absorption of sound: update. J. Acoust. Soc. Am. 88, 2019–2021.
Bishop, I.D., Stock, C., 2010. Using collaborative virtual environments to plan wind energy installations. Renew. Energy 35 (10), 2348–2355.
Bishop, I.D., 2011. Landscape planning is not a game: should it be? Landsc. Urban Plan. 100 (4), 390–392.
Chessell, C., 1977. Propagation of noise along a finite impedance boundary. J. Acoust. Soc. Am. 62, 825–834.
Crocker, M.J., 2007. Handbook of Noise and Vibration Control. John Wiley & Sons.
Daigle, G., Piercy, J., Embleton, F., 1978. Effects of atmospheric turbulence on the interference of sound waves near a hard boundary. J. Acoust. Soc. Am. 64, 622–630.
Daigle, G., 1979. Effects of atmospheric turbulence on the interference of sound waves above a finite impedance boundary. J. Acoust. Soc. Am. 65, 45–49.
Deal, W.F., 2010. Wind power: an emerging energy resource. Technol. Eng. Teach. 70, 9–15.
de La Beaujardière, J., 2002. Web Map Service Implementation Specification. OpenGIS® Implementation Specification, 1.1.1, OGC 01-068r3. Open Geospatial Consortium, Inc.. https://portal.opengeospatial.org/files/?artifact_id=1081&version=1&format=pdf
Delany, M., Bazley, E., 1970. Acoustical properties of fibrous absorbent materials. Appl. Acoust. 3 (2), 105–116.
Embleton, T., Piercy, J., Daigle, G.A., 1983. Effective flow resistivity of ground surfaces determined by acoustical measurements. J. Acoust. Soc. Am. 74, 1239–1244.
EU Directive, 2009. Directive 2009/28/EC of the European Parliament and of the Council of 23 April 2009 on the promotion of the use of energy from renewable sources and amending and subsequently repealing Directives 2001/77/EC and 2003/30. Off. J. EU, Eur. Comm. 5, 16–62.
EWEA, 2015. European Wind Energy Association: Wind in Power: 2014 European Statistics (Retrieved 2014-11-05).
Evans, A., Vladimir, S., Evans, T.J., 2009. Assessment of sustainability indicators for renewable energy technologies. Renew. Sustain. Energy Rev. 13 (5), 1082–1088.
Filios, A.E., Tachos, N.S., Fragias, A.P., Margaris, D.P., 2007. Broadband noise radiation analysis for an HAWT rotor. Renew. Energy 32 (9), 1497–1510.
Forrest, T.G., 1994. From sender to receiver: propagation and environmental effects on acoustic signals. Am. Zoologist 34 (6), 644–654.
Geertman, S., Stillwell, J., 2012. Planning support systems in practice. Springer Science & Business Media.
Goodall, J.L., Robinson, B.F., Castronova, A.M., 2011. Modeling water resource systems using a service-oriented computing paradigm. Environ. Model. Softw. 26 (5), 573–582.
Gregory, J., 2009. Game Engine Architecture, second ed. CRC Press, pp. 28–38.
Grosveld, F.W., Shepherd, K.P., Hubbard, H.H., 1995. Measurement and prediction of broadband noise from large horizontal axis wind turbine generators. Wind Turbine Technol. 1, 211–220.
Groth, T.M., Vogt, C., 2014. Residents' perceptions of wind turbines: an analysis of two townships in Michigan. Energy Policy 65, 251–260.
Hall, N., Ashworth, P., Devine-Wright, P., 2013. Societal acceptance of wind farms: analysis of four common themes across Australian case studies. Energy Policy 58, 200–208.
Herwig, A., Paar, P., 2002. Game engines: tools for landscape visualization and planning. Trends GIS Virtualization Environ. Plan. Des. 161, 172.
Jallouli, J., Moreau, G., 2009. An immersive path-based study of wind turbines' landscape: a French case in Plouguin. Renew. Energy 34 (3), 597–607.
Jobert, A., Laborgne, P., Mimler, S., 2007. Local acceptance of wind energy: factors of success identified in French and German case studies. Energy Policy 35 (5), 2751–2760.
Johnson, M., Raspet, R., Bobak, M., 1987. A turbulence model for sound propagation from an elevated source above level ground. J. Acoust. Soc. Am. 81 (3), 638–646.
Kurze, U., Anderson, G., 1971. Sound attenuation by barriers. Appl. Acoust. 4, 35–53.
Kurze, U., 1971. In: Beranek, L.L. (Ed.), Noise and Vibration Control. Noise and Vibration Control. McGraw-Hill.
Maekawa, Z., 1968. Sound attenuation by screens. Appl. Acoust. 3 (1), 157–173.
Manwell, J., McGowan, J., Rogers, A., 2002. Wind Energy Explained: Theory, Design and Application. John Wiley, West Sussex, UK.
Masó, J., Pomakis, K., Julià, N., 2010. Web Map Tile Service Implementation Standard. OpenGIS® Implementation Standard, 1.0.0 : OGC 07-057r7. Open Geospatial Consortium, Inc.. http://portal.opengeospatial.org/files/?artifact_id=35326
Moriarty, P., Guidati, G., Migliore, P., 2005. Prediction of turbulent inflow and trailing-edge noise for wind turbines. Proc. 11th AIAA/CEAS Aeroacoustics Conf. (Monterey, Canada). AIAA Paper 2881.
Nicolas, J., Berry, J., Daigle, G., 1985. Propagation of sound above a finite layer of snow. J. Acoust. Soc. Am. 77, 67–73.
O'Coill, C., Doughty, M., 2004. Computer game technology as a tool for participatory design. In: eCAADe2004. Architecture in the Network Society, Copenhagen, Denmark.
Oerlemans, S., Sijtsma, P., Méndez López, B., 2007. Location and quantification of noise sources on a wind turbine. J. Sound Vib. 299 (4), 869–883.
Oerlemans, S., Schepers, J., 2009. Prediction of wind turbine noise and validation against experiment. Acoustics 8, 555–584.
Pedersen, E., 2011. Health aspects associated with wind turbine noise—results from three field studies. Noise Control Eng. J. 59 (1), 47–53.
Piercy, J.E., Embleton, T.F.W., Sutherland, L.C., 1977. Review of noise propagation in the atmosphere. J. Acoust. Soc. Am. 61 (6), 1403–1418.
Pierpont, N., 2009. Wind Turbine Syndrome: a Report on a Natural Experiment. K-Selected Books, Santa Fe, NM, USA.
Prospathopoulos, J.M., Voutsinas, S.G., 2007. Application of a ray theory model to the prediction of noise emissions from isolated wind turbines and wind parks. Wind Energy 10, 103–119.
Saidur, R., Rahim, N.A., Islam, M.R., Solangi, K.H., 2011. Environmental impact of wind energy. Renew. Sustain. Energy Rev. 15 (5), 2423–2430.
SER, 2013. Energieakkoord Voor Duurzame Groei. http://www.ser.nl/~/media/files/internet/publicaties/overige/2010_2019/2013/energieakkoord-duurzame-groei/energieakkoord-duurzame-groei.ashx.
Stock, C., Bishop, I.D., O'Connor, A.N., Chen, T., Pettit, C.J., Aurambout, J.P., 2008. SIEVE: collaborative decision-making in an immersive online environment. Cartogr. Geogr. Inf. Sci. 35 (2), 133–144.
Strobl, J., 2006. Visual interaction: enhancing public participation. 7th Int. Conf. Inf. Technol. Landsc. Archit. Trends Knowledge-Based Landsc. Model.
Tadamasa, A., Zangeneh, M., 2011. Numerical prediction of wind turbine noise. Renew. Energy 36, 1902–1912.
Tippett, J., 2005. The value of combining a systems view of sustainability with a participatory protocol for ecologically informed design in river basins. Environ. Model. Softw. 20 (2), 119–139.
Vitolo, C., Elkhatib, Y., Reusser, D., Macleod, C.J., Buytaert, W., 2015. Web technologies for environmental big data. Environ. Model. Softw. 63, 185–198.
Vretanos, P.A., 2005. Web Feature Service Implementation Specification. OpenGIS® Implementation Specification, 1.1.0, OGC 04-094. Open Geospatial Consortium, Inc.. https://portal.opengeospatial.org/files/?artifact_id=8339
Wagner, S., Bareiss, R., Guidati, G., 1996. Wind Turbine Noise. Springer, Berlin, Germany.
2020 climate & energy package, 2009. European Commission, Climate Action, Package. http://ec.europa.eu/clima/policies/strategies/2020/index_en.htm (last accessed 11.02.16).